Late Quaternary environmental change in the interior South American tropics: new insight from leaf wax stable isotopes

Kyrstin L. Fornace,[a,b*] Bronwen S. Whitney,[c] Valier Galy,[b] Konrad A. Hughen,[b] Francis E. Mayle[d]

a. MIT/WHOI Joint Program in Oceanography/Applied Ocean Science and Engineering, Cambridge, MA 02139, USA.
b. Department of Marine Chemistry and Geochemistry, Woods Hole Oceanographic Institution 266 Woods Hole Rd, Woods Hole, MA 02543, USA.
c. Department of Geography, Northumbria University Newcastle, Ellison Place, Newcastle-Upon-Tyne, NE1 8ST, UK.
d. Department of Geography and Environmental Science, University of Reading, Whiteknights, Reading, RG6 6AB, UK.

*corresponding author: kfornace@whoi.edu

Abstract

Stable isotope analysis of leaf waxes in a sediment core from Laguna La Gaiba, a shallow lake located at the Bolivian margin of the Pantanal wetlands, provides new perspective on vegetation and climate change in the lowland interior tropics of South America over the past 40,000 years. The carbon isotopic compositions ($\delta^{13}C$) of long-chain *n*-alkanes reveal large shifts between C_3- and C_4-dominated vegetation communities since the last glacial period, consistent with landscape reconstructions generated with pollen data from the same sediment core. Leaf wax $\delta^{13}C$ values during the last glacial period reflect an open landscape composed of C_4 grasses and C_3 herbs from 41-20 ka. A peak in C_4 abundance during the Last Glacial Maximum (LGM, ~21 ka) suggests drier or more seasonal conditions relative to the earlier glacial period, while the development of a C_3-dominated forest community after 20 ka points to increased humidity during the last deglaciation. Within the Holocene, large changes in the abundance of C_4 vegetation indicate a transition from drier or more seasonal conditions during the early/mid-Holocene to wetter conditions in the late Holocene coincident with increasing austral summer insolation. Strong negative correlations between leaf wax $\delta^{13}C$ and δD values over the entire

record indicate that the majority of variability in leaf wax δD at this site can be explained by variability in the magnitude of biosynthetic fractionation by different vegetation types rather than changes in meteoric water δD signatures. However, positive δD deviations from the observed $\delta^{13}C$-δD trends are consistent with more enriched source water and drier or more seasonal conditions during the early/mid-Holocene and LGM. Overall, our record adds to evidence of varying influence of glacial boundary conditions and orbital forcing on South American Summer Monsoon precipitation in different regions of the South American tropics. Moreover, the relationships between leaf wax stable isotopes and pollen data observed at this site underscore the complementary nature of pollen and leaf wax $\delta^{13}C$ data for reconstructing past vegetation changes and the potentially large effects of such changes on leaf wax δD signatures.

Keywords: Pantanal, leaf wax, compound-specific stable isotopes, South American Summer Monsoon, last glacial period, Holocene

1. Introduction

Characterizing the controls on South American Summer Monsoon (SASM) dynamics on geological timescales provides critical context for investigating present and future trends in South American tropical climate. Changes in the distribution and intensity of SASM precipitation can alter hydrologic and vegetation patterns across much of the South American continent with potentially significant ramifications for both the global carbon cycle and climate system. An increasingly coherent picture of late Quaternary SASM behavior has begun to emerge from a number of records of SASM precipitation from the Central Andes, western Amazonia and southern Brazil (Cruz et al., 2005; Wang et al., 2007; Mosblech et al., 2012; Kanner et al., 2012; Cheng et al., 2013; Fornace et al., 2014). These records indicate that

generally wet conditions prevailed during the Last Glacial Maximum (LGM) and late glacial period, followed by a shift towards drier conditions in the early/mid-Holocene. After this dry period, SASM precipitation has gradually increased into the present, a trend widely attributed to increasing summer insolation through the Holocene (e.g., Bird et al., 2011).

Missing from this discussion of past SASM trends are critical records from the interior tropics, where climate archives such as lacustrine sediments or speleothems rarely extend back to the last glacial period. Available pollen records from several sites in the southern Amazon Basin point to drier conditions during the last glacial period (Mayle et al. 2000; Burbridge et al., 2004), suggesting a disconnect between the interior tropics and other regions. Several recent studies have focused on reconstructing hydrologic conditions in the Pantanal, a large wetland expanse primarily located in the Mato Grosso do Sul region of Brazil and roughly equidistant between the well-studied Central Andes and southern Brazil regions (Metcalfe et al., 2014; Whitney et al., 2011; Whitney and Mayle, 2012; McGlue et al., 2012). Evidence from pollen, diatoms and other biological proxies in a continuous ~45,000-year sediment record from Laguna La Gaiba (LLG) suggest drier and cooler conditions in the Pantanal during the last glacial period (Metcalfe et al., 2014; Whitney et al., 2011). During the Holocene, hydrologic patterns in the Pantanal appear to be consistent with other SASM records, with a relatively dry early/mid-Holocene followed by wetter conditions in the late Holocene (Metcalfe et al., 2014; Whitney et al., 2011; Whitney and Mayle, 2012; McGlue et al., 2012). However, existing evidence of hydrologic change in the Pantanal derived from past biota assemblages is complicated by complex or non-specific relationships between climate and species distributions. Independent climate proxies can thus offer further insight into landscape and hydrologic changes in this region and allow for more robust comparison with other tropical South American records.

In this study, we use stable isotope analysis of terrestrial biomarkers in LLG sediments to better characterize environmental changes at this site and regional SASM precipitation patterns during glacial and interglacial periods. Specifically, we analyze the carbon ($\delta^{13}C$) and hydrogen (δD) isotopic compositions of leaf waxes, a suite of long-chain lipids produced by terrestrial and emergent aquatic vascular plants now commonly employed to reconstruct past climate change in a wide range of environments (see review by Eglinton and Eglinton, 2008). We use C_{27}-C_{33} *n*-alkane $\delta^{13}C$ to reconstruct changes in the distribution of C_3 vs. C_4 vegetation, which is controlled by a range of climatic factors, including atmospheric CO_2 concentration, temperature, and water availability (Ehleringer et al., 1997). In particular, the prevalence of C_4 vegetation at warm tropical or subtropical sites is often linked to drier or more seasonal conditions (Still, 2003). Leaf wax δD has been shown to reliably track trends in meteoric water δD, providing direct information about climatic trends. However, the relationship between meteoric water and leaf wax δD can be influenced by a number of secondary effects, including soil evaporation and leaf transpiration processes as well as variability in biosynthetic fractionation among different vegetation types (see review by Sachse et al., 2012). The combination of leaf wax $\delta^{13}C$ and δD data with detailed pollen information from the same sediment core thus provides a unique opportunity to investigate the fidelity of pollen and leaf wax $\delta^{13}C$ vegetation reconstructions and address outstanding questions about the effects of vegetation change on leaf wax δD signatures.

2. Background

2.1 Study site description

The Pantanal is a large (140,000 km^2) expanse of wetlands situated in a low-lying sedimentary basin in central western Brazil with smaller areas in Bolivia and Paraguay (Figure 1,

2). The landscape of the basin mostly consists of large fluvial fans deposited by a number of rivers that flow from upland regions to the western side of the basin, eventually converging with the north-south flowing Paraguay River (Assine et al., 2015). Laguna La Gaiba (LLG, 17.75°S, 57.58°W) is a large, shallow lake (maximum area and depth of ~100 km^2 and 4-6 m, respectively) located along the upper Paraguay River (Figure 2). The lake is also connected to the Corixo Grande River, which flows along the western border of the Pantanal basin towards the lake. In the present day, the lowland areas immediately surrounding the lake are populated by wetland and savanna vegetation found throughout the seasonally or permanently flooded grasslands of the Pantanal basin (Whitney et al., 2011). The margins of the lake are confined by bordering highland areas populated by seasonally dry tropical forest (SDTF).

The LLG sediment record is largely continuous over the past ~40 kyr, as supported by 17 macrofossil and two sediment radiocarbon dates over 38 kyr (Whitney et al., 2011). However, a ~5-10-fold increase in the LLG sedimentation rate at ~13 ka indicates a dramatic increase in sediment input to the lake (Whitney et al., 2011; Metcalfe et al., 2014). This change could be related to large-scale reorganization of Pantanal basin drainage pathways thought to be driven by hydrologic change around the onset of the Holocene (Assine and Soares, 2004). There is clear geomorphological evidence that the Paraguay River has shifted eastward across its fluvial fan upstream of LLG multiple times in the past, although the absolute timing of these shifts is not known (Assine and Silva, 2009) (Figure 2). In previous configurations, the Paraguay River likely would have converged with the Corixo Grande River at a point further north than LLG. Thus, the establishment of the modern configuration of the Paraguay River could have increased sediment delivery to LLG through increased erosion and/or creation of a more direct connection between the river and the lake. However, such a change probably did not significantly affect the water

balance of LLG since in pre-modern configurations, water would presumably still have been channeled from the Paraguay headwaters to LLG through the Corixo Grande, which flows into the lake along a route more constrained by local topography (Figure 2). Evidence of lake level rise between ~13-12 ka thus supports a mechanism of landscape reshaping driven by changes in regional hydroclimate (Whitney et al., 2011).

2.2 Overview of regional climate patterns

The modern climate of the Pantanal is highly seasonal, with the majority of annual precipitation (1000-1500 mm) falling between November and March and little precipitation during the winter months (Hamilton, 2002). Temperatures in the Pantanal range from highs of 40-44°C in spring and summer months to occasional lows near freezing in the winter, with a mean annual temperature of 25°C (Alho, 2005). Summer precipitation causes widespread seasonal flooding, which generally progresses from north to south and can result in simultaneous inundation of >75% of the total area of the Pantanal. Wet season precipitation is associated with the development of the SASM in austral spring (Zhou and Lau, 1998). During the mature phase of the monsoon (December-February), strengthened easterly trade winds increase moisture transport from the tropical Atlantic into equatorial South America, and widespread deep convection develops throughout the southern Amazon Basin (Figure 1). The development of the South American Low Level Jet carries moisture in a general arc along the eastern Andean flank and to the southeast towards the Pantanal and subtropical Brazil (Garreaud et al., 2009). After the demise of the monsoon in austral autumn, the zone of maximum precipitation retreats to the northern hemisphere South American tropics, resulting in little precipitation in the Pantanal outside of the monsoon season.

The influence of SASM precipitation is reflected in the large seasonal signal in the hydrogen isotopic composition of precipitation (δD_p) that falls in the Pantanal. According to 1961-1987 data from the Cuiabá IAEA station (15.60°S, 56.10°W) on the northern edge of the Pantanal, precipitation δD (δD_p) is significantly lower in the monsoon season (average DJFM δD_p = -41‰ VSMOW) than during the dry season (average JJAS = +4‰ VSMOW) with a weighted annual average of -31‰. In the southern hemisphere South American tropics, the dominant climatic influence on δD_p is the amount of precipitation that falls along the SASM trajectory from the Amazon Basin to the site of interest (Vuille et al., 2003; Vuille and Werner, 2005). Increased precipitation along this trajectory results in more negative δD_p values through Rayleigh-type fractionation. Higher local precipitation can also result in more D-depleted precipitation due to the "amount effect" (Dansgaard, 1964), although upstream and local precipitation intensity may not necessarily act in concert given the significant spatial variability in SASM rainfall (Vuille and Werner, 2005).

3. Methods

3.1 Sediment collection

Sediment samples (1-2 cm) were taken from overlapping piston cores LLG1 (5.6 m) and LLG1a (4.8 m) and a 1m surface core LGS raised from the deepest part of LLG (see Whitney et al., 2011 for further details on sediment core retrieval and sediment description). Sample ages were assigned using depth-age models developed by Whitney et al. (2011) based on radiocarbon dating of plant macrofossils and sedimentary organic matter. Surface sediment samples were also collected from the core site and at the flooded wetland margin of the lake that lies along the course of the Paraguay River.

3.2 Sample preparation

n-Alkanes were extracted and purified from sediment samples as detailed in supplementary material. Average chain length (ACL, *n*-C_{25}–C_{35} odd carbon numbers) was calculated according to the formula:

$$ACL_{25-35} = \sum_{n=25,27...}^{35} n * [C_n] / \sum_{n=25,27...}^{35} [C_n]$$

The carbon preference index (CPI) was calculated according to the formula (Marzi et al., 1993):

$$CPI = \frac{([C_{25}] + [C_{27}] + [C_{29}] + [C_{31}] + [C_{33}]) + ([C_{27}] + [C_{29}] + [C_{31}] + [C_{33}] + [C_{35}])}{2([C_{24}] + [C_{26}] + [C_{28}] + [C_{30}] + [C_{32}])}$$

3.3 Compound-specific stable isotope analysis

The $\delta^{13}C$ values of individual *n*-alkanes were measured in triplicate on a Finnegan Delta^{plus} isotope ratio mass spectrometer (IRMS) coupled to an HP 6890 gas chromatograph (GC) via a combustion interface operated at 850°C. Several pulses of a CO_2 reference gas were inserted during each run and used to correct for instrument drift. The reference gas was calibrated prior to sample measurement by running multiple external standards at a range of concentrations. Average precision of sample replicates was 0.2‰ (1σ). Estimated average accuracy was ≤ 0.3‰.

The δD values of individual *n*-alkanes were measured on a Thermo Scientific DeltaV^{Plus} IRMS coupled to an Agilent 6980 GC via a pyrolysis interface operated at 1440°C. Each sample was analyzed in duplicate with the exception of two out of 40 total samples that were concentration-limited and measured once. The H_3^+ factor (Sessions et al., 2001) was measured daily and was under 2 ppm/mV throughout the measurement period. Peaks of a propane

reference gas were inserted at several points before and after analytes during each run and used as internal calibration standards. Variability in instrumental fractionation was accounted for by routinely injecting an external standard mix containing 8 fatty acid methyl and ethyl esters of known δD (F8 mixture, A. Schimmelmann, Indiana University) and adjusting the reference propane δD value to minimize the average offset between the known and measured δD values of the F8 compounds. Average precision of sample replicates was 2.5‰ (1σ). Estimated average accuracy was 4‰ based on daily measurements of the F8 mixture.

4. Results

n-Alkanes in LLG sediments are dominated by long chain lengths (*n*-C_{25}-C_{35}) with consistently high carbon preference index (CPI) values found throughout the core (range = 2.9-4.5). Such a distribution is typical of fresh vegetation and renders any significant contamination from oil or other fossil carbon sources unlikely (Bray and Evans, 1961; Eglinton and Hamilton, 1967). $\delta^{13}C$ values for C_{27}-C_{33} *n*-alkanes and δD values for C_{29}-C_{33} *n*-alkanes, as well as $ACL_{25\text{-}35}$ values, are shown in Figure 3. All data will also be made available online in the NOAA/NCEI Paleoclimatology Database. We restrict our discussion of δD variability to *n*-C_{29}-C_{33} data, as considerable differences between *n*-C_{27} and *n*-C_{29}-C_{33} δD values during the Holocene suggest significant input from a different *n*-alkane source. One possible source is submerged aquatic plants, which have been found to produce significant amounts of *n*-alkanes in the n-C_{23}-C_{27} range (e.g., Do Amaral et al., 1990; Ficken et al., 2000). This effect is not apparent in *n*-C_{27} $\delta^{13}C$ data, perhaps due to similar $\delta^{13}C$ signatures of submerged aquatic plants compared to other vegetation. All reported δD values have been corrected for ice volume effects on ocean isotopic composition using reconstructions of ocean surface water $\delta^{18}O$ from Bintanja et al. (2005) scaled by a factor

of 8 (i.e., meteoric water line slope). Ranges for $\delta^{13}C$ and δD values over the record are -21.5 to -35.8‰ and -157 to -195‰, respectively.

4.1 Surface sediment samples

n-Alkanes in two surface samples from the core site and wetland margin of LLG (see Figure 2 for locations) show relatively uniform $\delta^{13}C$ values between -32.1 and -29.3‰ (Table 1). δD values from the core site sample are slightly higher (~8-10‰) than those in the lake margin sample.

4.2 Glacial samples (~41-12 ka)

From 41-20 ka, there is a large offset (~3-4 ‰) between relatively high *n*-C_{33} $\delta^{13}C$ values (-23 to -25 ‰) and shorter *n*-alkane $\delta^{13}C$ values. After a local minimum at ~37.5 ka, all chain lengths show a steady increase in $\delta^{13}C$ into the LGM. δD values for all chain lengths remain relatively constant from 41-20 ka, although C_{29} and C_{31} *n*-alkanes show slightly higher δD values around ~33-29 ka. There is a large spread in δD values (>20‰) between different *n*-alkanes, with mean glacial δD value decreasing with increasing chain length. High $ACL_{25\text{-}35}$ values are found throughout the full glacial period, driven by relatively large amounts of *n*-C_{33}.

The late glacial period (~20-12 ka) is marked by a sustained period of low $\delta^{13}C$ values (< -30‰) in all chain lengths, with mean $\delta^{13}C$ values increasing with chain length. As in the full glacial section, mean δD values decrease with increasing chain length, but after 20 ka, there is a narrower spread of δD values across different chain lengths. After higher δD values at ~19 ka, δD values for all chain lengths show reduced variability from ~17.5-12.5 ka. $ACL_{25\text{-}35}$ values are markedly lower than in the full glacial period and remain relatively constant from 20-12 ka.

4.3 Holocene samples (~12 ka–present)

Between ~12.7 and 11.6 ka, δD values for all *n*-alkane chain lengths decrease sharply by ~10-20‰, coincident with a ~3-5‰ increase in $\delta^{13}C$ values. $\delta^{13}C$ values continue to rise further into a mid-Holocene maximum from 8.9-6.4 ka ($\delta^{13}C$ for all compounds ≥ -26‰) and then steadily decrease into the present. In contrast to the glacial period, there is no systematic offset of $\delta^{13}C$ values by chain length. δD values are generally lower during the Holocene compared to the late glacial period except for two periods of higher values during the mid-Holocene (~7.6 ka) and in the late Holocene (~2.2-0 ka). $ACL_{25\text{-}35}$ values further decrease during the Holocene as the abundances of shorter chain lengths (*n*-C_{25}, *n*-C_{27}) increase relative to those of longer chain length compounds.

5. Discussion

5.1 Modern leaf wax $\delta^{13}C$ at LLG

Leaf wax $\delta^{13}C$ values from surface sediment samples collected at the core site and near the Paraguay River establish a context for interpreting past changes in C_3 and C_4 vegetation distributions. We assume any contributions of waxes from crassulacean acid metabolism (CAM) plants at LLG are minor since CAM plants are relatively minor components of the vegetation cover in tropical savannas and forests (Lüttge, 2010) and generally not found in Pantanal macrophyte populations (Do Prado et al., 1994). Extensive analyses of diverse vegetation types have shown that C_3 plants produce leaf waxes with $\delta^{13}C$ values that range from -30 to -40‰ while those using the C_4 pathway produce much more enriched waxes (-15 to -23‰) (e.g., Chikaraishi and Naraoka, 2003; Garcin et al., 2014). The relatively low $\delta^{13}C$ values (-29.3 to -32.1‰) found at the core site thus point to a mostly C_3 vegetation community at LLG in the

present day. Similarly low $\delta^{13}C$ values (-29.8 to -31.3‰) found in sediment from the LLG wetland margin along the Paraguay River show that the proximity of large areas of SDTF to LLG is not solely responsible for the low $\delta^{13}C$ signature of *n*-alkanes at the core site. We thus conclude that the seasonally flooded savannas and wetlands upstream of LLG support mostly C_3 vegetation with smaller amounts of C_4 plants at present.

This conclusion is consistent with a number of vegetation surveys of the Pantanal (Pott et al., 2011; Schessl, 1999; Alho, 2005). The lower lying areas of the Pantanal are permanently or seasonally flooded grasslands, while higher elevations are saturated and/or occasionally inundated during the wet season and experience drought during the dry season. Woody vegetation (C_3) is generally found in these higher elevation areas, as well as in gallery forests along rivers and streams (Alho, 2005). Herbaceous vegetation in the Pantanal includes a wide range of C_3 and C_4 terrestrial and aquatic species. In tropical flooded savannas, flooding depth and duration have been found to be major controls on the C_3/C_4 distribution of grasses, with the proportion of C_3 grasses increasing with the extent of flooding (Medina and Motta, 1990; Knapp and Medina, 1999). In the Pantanal, C_4 grasses (e.g., *Elyonurus miticus, Axonopus purpusii*) dominate in higher elevation areas that never or rarely flood as well as in seasonally flooded grasslands during the dry season (Alho, 2005), while aquatic or semi-aquatic C_3 grasses (e.g. *Panicum laxum*, *Hymenachne amplexicaulis*) grow in wet or flooded areas (Rodela et al., 2007). Isotopic studies also show that most macrophytes (both grasses and forbs) in inundated regions use the C_3 pathway (Fellerhoff et al., 2003; Wantzen et al., 2002). Thus, considering the mostly-C_3 signature of modern leaf waxes, the widespread flooding of the Pantanal at present allows contributions from both C_3 grasses/macrophytes and trees to outweigh those from C_4 grasses.

5.2 Past vegetation change at LLG

The very large range of $\delta^{13}C$ values (-35.3 to -21.5‰) in the LLG record suggests the site experienced a wide spectrum of C_3-dominated to C_4-dominated plant communities over the past 40 kyr. Comparison of $\delta^{13}C$ changes to detailed pollen data provides additional perspective on vegetation patterns at LLG (Figure 4). The three major pollen zones described by Whitney et al. (2011) are clearly delineated in the LLG $\delta^{13}C$ record with large shifts at ~20 and ~12 ka, pointing to general coherence between the two records.

Closer inspection of the $\delta^{13}C$ trends within different periods yields further insight into vegetation patterns at LLG and controls on leaf wax $\delta^{13}C$. During the full glacial period (41-20 ka), *n*-alkane $\delta^{13}C$ values reflect a mixed C_3/C_4 community. While the estimated 1-4°C cooler temperatures during the last glacial period (Whitney et al., 2011; Punyasena et al., 2008) would tend to promote the growth of C_3 vegetation, this effect was likely counteracted at least in part by lower glacial pCO_2, which decreased the temperature threshold for C_4 favorability and increased the sensitivity of C_3 plants to water stress (Ehleringer and Monson, 1993; Ehleringer et al., 1997). A long-term increasing trend in $\delta^{13}C$ values of all *n*-alkanes after ~35 ka also shows that the abundance of C_4 vegetation peaked during the LGM, suggesting increased water stress at this time relative to the earlier glacial period. Positive linear correlations between $\delta^{13}C$ values and graminoid (*Cyperaceae* + *Poaceae*) pollen abundance indicate that C_3 herbs and C_4 grasses were likely the two major vegetation groups present from 41-20 ka (Table 2). $ACL_{25\text{-}35}$ values also show strong correlations to graminoid pollen abundance and individual *n*-alkane $\delta^{13}C$ values, indicating that $ACL_{25\text{-}35}$ was also controlled by mixing between a C_4 grass group that produced longer *n*-alkanes and C_3 herbs with relatively shorter *n*-alkanes (Table 2). The ~3-4‰ offset

between *n*-C_{33} and shorter *n*-alkane $\delta^{13}C$ values further shows that C_4 grasses were the dominant source of *n*-C_{33}.

After 20 ka, there is a sharp drop in $\delta^{13}C$ values across all chain lengths coincident with the rise of floodplain trees around LLG indicated by pollen data. The development of a C_3-dominated vegetation community before the glacial-interglacial rise of pCO_2 suggests abundant water availability after 20 ka. As observed in the full glacial period, $\delta^{13}C$ values increase with increasing chain length, indicating larger contributions from C_4 grasses at the longest chain lengths. However, even though pollen data show similar or increased abundance of grasses during the late glacial compared to the full glacial period, the influence of C_4 grasses on leaf wax $\delta^{13}C$ is diminished. The discrepancy between pollen and leaf wax data can be explained by either (1) an increasing proportion of C_3 grasses due to alleviation of water stress or (2) differences in the rates of production and/or transport mechanisms of pollen and waxes by different vegetation types. In support of the latter explanation, wind-pollinated grass species have been observed in some cases to be overrepresented by pollen data compared to floodplain tree species, which can have low pollen dispersal rates (Burn et al., 2010; Bush, 2002). Moreover, there is strong evidence that floodplain trees formed a fringing community on the lake shores (Whitney et al., 2011), suggesting the leaf wax $\delta^{13}C$ signal was likely dominated by floodplain tree input due to their proximity to the lake.

A sharp increase in $\delta^{13}C$ values across all chain lengths from ~12.7-11.6 ka is similar in timing to the observed increase in sedimentation rate at ~13 ka and lake level rise between ~13-12 ka (Whitney et al., 2011). While the source region for leaf waxes was likely similar before and after any hydrologic reorganization at this time (see Section 2.1), increased sediment input to the lake likely increased the proportion of waxes derived from the Paraguay River catchment.

Furthermore, the large increase in lake level destroyed most of the fringing floodplain tree community around LLG (Whitney et al., 2011), eliminating one source of C_3 waxes close to the core site. Thus, the increase in $\delta^{13}C$ values could reflect vegetation change (i.e., removal of floodplain trees, establishment of mixed C_3/C_4 wetland vegetation communities in the lowland regions of the Paraguay River catchment) and/or increased fluvial input of leaf waxes to LLG from previously established wetland communities in the Paraguay River catchment. Given the evidence of widespread hydrologic change throughout the Pantanal basin in the early Holocene (Assine and Soares, 2004), it is likely a combination of all factors.

In contrast to the glacial period, leaf wax $\delta^{13}C$ during the Holocene shows significant changes independent of changes in pollen composition. After the initial increase of ~4-6‰ at the beginning of the Holocene, $\delta^{13}C$ values reach the highest values of the record in the mid-Holocene. During the mid-Holocene, all *n*-alkanes have $\delta^{13}C$ values greater than -26‰ with little or no offset between different chain lengths, indicating a C_4-dominated community. Pollen data show a significant presence (~20-30% of major vegetation pollen) of SDTF near LLG at this time, and a strong negative correlation between $ACL_{25\text{-}35}$ and SDTF pollen abundance ($r^2 = 0.87$, $p < 0.0001$) provides evidence that SDTF was indeed contributing to the leaf wax pool over the entire Holocene. This requires nearly all remaining herbaceous vegetation to have been C_4 plants in order to produce such high $\delta^{13}C$ values in the mid-Holocene. Since the modern flooding regime in the Pantanal is associated with majority C_3 vegetation, this suggests more seasonal or drier conditions during the mid-Holocene reduced the extent/duration of flooding and promoted widespread growth of C_4 grasses. This conclusion is further supported by evidence of lower lake level, minima in rainforest species and the increased abundance of drought-tolerant trees from 10-3 ka (Whitney et al., 2011; Whitney and Mayle, 2012). After the mid-Holocene, $\delta^{13}C$ values

decrease steadily into the present, reflecting increasing contributions from C_3 vegetation. Since the abundance of SDTF pollen does not dramatically change in the late Holocene, we posit that the decreasing trend in $\delta^{13}C$ is due to increasing flooding, which resulted in the rise of C_3 macrophytes and other C_3 vegetation (e.g., gallery forest) common in the extensively flooded regions of the modern Pantanal.

5.3 Interpreting the LLG δD record

The similarities between the LLG δD and $\delta^{13}C$ records (i.e., distinct shifts in δD values and distribution of δD values across chain length at pollen zone transitions) provide the first indication that vegetation composition may be a significant influence on leaf wax δD at this site (Figure 3). The likely influence of changing vegetation is made clear by comparing measured δD and $\delta^{13}C$ values for *n*-C_{29} -C_{33} (Figure 5). Leaf wax δD and $\delta^{13}C$ values show a consistent negative relationship across all time periods, contradicting the expected association of low δD values (i.e., more intense monsoon/higher humidity) and low $\delta^{13}C$ values (i.e., C_3 vegetation) if climatic factors were the main control on δD. Thus, much of the variability in LLG δD can be explained by mixing between C_3 herb and C_4 grass end members from 41-20 ka and C_3 tree/macrophyte and C_4 grass end members from 20-0 ka. More negative δD values for C_4 grasses are in line with the larger *n*-alkane/water fractionation factors ($\varepsilon_{l/w}$) previously found for grasses compared to forbs and trees (Sachse et al., 2012). However, assuming a constant source water δD, the large difference (~40-50‰) between δD values corresponding to C_3 and C_4 end members requires a larger range in $\varepsilon_{l/w}$ values for different vegetation types than the <20‰ range in average $\varepsilon_{l/w}$ values reported for forbs, trees and C_4 graminoids in the Sachse et al. (2012)

compilation. Nevertheless, a ~50‰ range in $\varepsilon_{l/w}$ is quite reasonable given the large variability of published values for different taxa within the same vegetation groups.

Significant correlations between graminoid pollen abundance and *n*-C_{29} and *n*-C_{31} leaf wax δD values across the entire record further support a relationship between vegetation and leaf wax δD (Figure 6). These results are also consistent with the strong relationship between δD and $\delta^{13}C$ as any C_4 plants present at LLG are likely graminoids. The lack of significant correlation between *n*-C_{33} δD and graminoid pollen abundance is likely because *n*-C_{33} is predominantly produced by graminoids, while other compounds provide better averages of total vegetation.

While vegetation effects appear to dominate the δD signal at LLG, there is also some evidence of climatic influence on leaf wax δD in the distinct $\delta^{13}C$-δD trends for 41-20 ka and 20-0 ka (Figure 5). These trends have similar slopes but are offset by ~10‰ in δD, suggesting an additional influence on leaf wax δD independent of vegetation change. This influence could be a change in source water δD resulting from changes in soil evaporation/leaf transpiration processes (e.g., Kahmen et al., 2013) or in the initial δD_p value. We note that the 20-0 ka regression excludes the set of values corresponding to 7.6-6.4 ka, which appear to plot separately from other 20-0 ka points. The statistical significance of the difference between 7.6-6.4 ka and other 20-0 ka data was confirmed with a one-way ANOVA test of residuals from a linear regression of all 20-0 ka δD and $\delta^{13}C$ data ($p < 0.0001$). However, calculated slopes for 7.6-6.4 ka and other 20-0 ka $\delta^{13}C$-δD trends are statistically identical within uncertainties (2σ level).

If the offset between 41-20 ka and 20-0 ka trends is in fact the result of source water δD differences, normalizing δD values for vegetation change could allow extraction of some climatic information. Therefore, we removed $\delta^{13}C$-δD trends by normalizing all δD values to a

hypothetical pure C_4 grass endmember (i.e., the vegetation type common to both Holocene and glacial periods) with $\delta^{13}C = -22‰$ using the formula:

$$\delta D_{vn} = \delta D_o - m(\delta^{13}C_o + 22)$$

where δD_o and $\delta^{13}C_o$ are the original δD and $\delta^{13}C$ values for each sample, m is the slope of the $\delta^{13}C$-δD correlation for either 20-0 or 41-20 ka, and δD_{vn} is the resulting vegetation-normalized δD value. We then subtract the mid-range of all δD_{vn} values to only consider relative changes in δD_{vn}. The resulting *n*-C_{29}-C_{33} δD_{vn} time series are shown in Figure 7. We caution that the amplitudes of δD_{vn} signals are small considering both analytical uncertainty and the potential for further vegetation or non-climatic influences on δD not accounted for by our $\delta^{13}C$-based normalization procedure. For example, the slight offset between *n*-alkane δD values for the two surface sediment samples, despite very similar $\delta^{13}C$ values (Table 1), could reflect further biosynthetic variability between different C_3 vegetation types. Despite all these caveats, periods of higher δD_{vn} from 35-19 ka and 7.6-6.4 ka are broadly consistent with drier/more seasonal conditions as indicated by leaf wax $\delta^{13}C$ and other proxies (Whitney et al., 2011; McGlue et al., 2012; Metcalfe et al., 2014). More positive δD_{vn} values during these periods could thus reflect source water enrichment due to lower local humidity and increased evapotranspiration and/or higher δD_p due to decreased local or regional precipitation intensity.

5.4 Paleoclimate implications

Our results provide further support for climate patterns described in previous studies at LLG but also reveal several new features in the climate history of the Pantanal (Figure 8). Leaf wax $\delta^{13}C$ values from 41-20 ka reflect an open landscape dominated by C_4 grass and C_3 herb communities. Lower glacial pCO_2 could contribute to the significant presence of C_4 grasses

(Ehleringer et al., 1997). The prevalence of C_4 grasses is also consistent with drier or more seasonal conditions during the last glacial period relative to the Holocene, as inferred from other proxies (Whitney et al., 2011) and observed at southern Amazon sites (Mayle et al., 2004). However, considering the complex influences of temperature and pCO_2 changes on C_3/C_4 distributions, as well as the likely hydrologic reorganization of the Pantanal at ~13-12 ka, we do not draw any conclusions about relative Holocene and glacial mean precipitation patterns from our data.

Within the glacial period, increased abundance of C_4 vegetation from 26-21 ka do suggest decreased humidity or increased seasonality during the LGM relative to the earlier glacial period. If δD_{vn} does reflect changes in source water δD signals, higher δD_{vn} values from 35-19 ka also support this conclusion. Relative drought during the LGM at LLG stands in contrast to clear evidence of wet conditions in the Central Andes (Baker et al., 2001; Fornace et al., 2014) at this time. However, speleothem records from western Amazonia do not show increased SASM intensity during the LGM as would be expected during a period of high austral summer insolation (Mosblech et al., 2012; Cheng et al., 2013). Model simulations of South American climate under LGM boundary conditions offer one possible explanation for the discrepancy between the Central Andes and lowland interior tropics. Using regional climate models, Cook and Vizy (2006) and Vizy and Cook (2007) found that a delayed onset of the monsoon under LGM conditions resulted in a longer dry season in the lowland tropics but also led to increased total annual precipitation in the Central Andes. Speleothem records from subtropical Brazil reveal a further complexity in glacial SASM dynamics as they generally indicate increasing monsoon precipitation from ~32 ka into the LGM, tracking increasing summer insolation (e.g., Cruz et al., 2005; Wang et al., 2007). These results suggest that circulation changes under LGM

boundary conditions increased moisture transport to the subtropics during the monsoon season but that this moisture was confined to regions south of LLG. Increases in LGM SASM precipitation may thus have been confined to the extremities of the SASM domain, similar to the "South American precipitation dipole" pattern defined by Cheng et al. (2013). Further modeling work, particularly in southern Brazil, would help to illuminate possible mechanisms for the variability in glacial-interglacial precipitation patterns throughout southern tropical South America.

After the LGM, vegetation at LLG went through a pronounced shift to a forested C_3-dominated landscape, which was present around the lake throughout the late glacial period (~19-13 ka). Whitney et al. (2011) attribute the rise of tropical trees at this time to deglacial warming, which pushed temperatures at LLG above the threshold for tropical forest, but it is likely that increased humidity during the last deglaciation also fostered the development of a C_3-dominated community despite lower pCO_2 levels. A sustained period of relatively low δD_{vn} values from ~17-10 ka is also consistent with increased humidity following the easing of LGM conditions. Wetter conditions at LLG could be related to increases in SASM precipitation throughout southern tropical South America from ~18-15 ka concurrent with Heinrich Event 1 (e.g., Blard et al., 2011; Mosblech et al., 2012; Wang et al., 2007), but the limits of the LLG record chronology and resolution preclude definitive identification of this event. Following a relatively stable late glacial period, the transition into the Holocene at LLG is marked by a dramatic shift to a mixed C_3/C_4 community from ~12.7 to 11.6 ka. This shift was likely the result of both hydrology-driven changes in the Pantanal landscape and increased leaf wax contribution from wetland regions.

The influence of orbital forcing on precessional timescales at LLG becomes evident during the Holocene (Figure 8). Leaf wax $\delta^{13}C$ and δD data point to drier conditions ca. 9-6 ka,

consistent with evidence of drier conditions throughout Amazonia during a period of generally low austral summer insolation (Mayle and Power, 2008). In the Central Andes, lake level records from Lake Titicaca also show a prolonged lowstand during the mid-Holocene (~8-4 ka) (Baker et al., 2001; Cross et al., 2000). These findings are consistent with the results of model simulations that show reduced SASM precipitation due to lower summer insolation in the mid-Holocene (Liu et al., 2004). However, the timing of vegetation change recorded by $\delta^{13}C$ at LLG appears to lag behind the insolation trend for the peak monsoon season (DJF), instead matching more closely the late summer (March) insolation curve. This trend stands in contrast to a number of isotopic records of SASM precipitation that generally show SASM intensity closely tracking DJF insolation (e.g., Bird et al., 2011). This discrepancy may be related to the different information contained in precipitation isotopes versus proxies directly tied to local hydrologic conditions. Precipitation isotopes are linked to intensity of monsoonal precipitation on a regional scale but do not necessarily reflect changes in the total amount or seasonality of local precipitation. Thus, widespread mid-Holocene drought may be related to a change in seasonality, namely a longer dry season, rather than a change in monsoon intensity during peak season. Based on the correlation between LLG $\delta^{13}C$ and March insolation, it is possible the magnitude of late summer insolation may be an important control on the timing of the monsoon demise and resulting seasonality. After the mid-Holocene, conditions at LLG became increasingly wet into the present, consistent with most records from SASM-dominated regions.

Overall, the climate history of LLG is distinct from most well-studied regions in southern tropical South America. While the Central Andes and southern Brazil experienced a relatively wet LGM, a trend towards drier conditions from ~35-21 ka at LLG suggests a reorganization of monsoon circulation under LGM boundary conditions that led to decreased precipitation in the

lowland interior tropics. We do not find any strong evidence of precessional orbital forcing at LLG during the last glacial period, consistent with several Central Andes and western Amazon records (Fornace et al., 2014; Cheng et al., 2013; Mosblech et al., 2012; Kanner et al., 2012) and in contrast to the strong precessional signal in southern Brazilian speleothem records (Cruz et al., 2005, Wang et al., 2007). During the Holocene, however, our record, along with most other SASM records, does support hydrologic change driven by precessional changes in insolation.

5.5 Implications for leaf wax isotope reconstructions

This study highlights the complementary nature of leaf wax stable isotopes and pollen data in assessing past environmental change. In the case of LLG, $\delta^{13}C$ data from multiple *n*-alkanes both confirm original vegetation reconstructions over the past 41 kyr and provide additional insight into past C_3/C_4 distributions, which are more directly tied to climate variables. In particular, $\delta^{13}C$ data allows differentiation of C_3 and C_4 grasses during the last glacial period and mid-Holocene, which carry very different implications for climate. In turn, pollen reconstructions of vegetation cover provide critical context for interpreting LLG $\delta^{13}C$ and differentiating between vegetation types with similar $\delta^{13}C$ signatures (i.e., C_3 herbs/trees).

At sites that likely experienced significant shifts in landscape cover, leaf wax δD records should be interpreted cautiously and whenever possible used in conjunction with other climate proxies. At LLG, a ~40-50‰ range in $\varepsilon_{l/w}$ values between different vegetation types likely overwhelmed changes in δD_p, but we were able to extract a putative hydrologic signal by removing $\delta^{13}C$-δD trends and thus accounting for vegetation change. However, if the magnitude of δD_p change exceeded the magnitude of vegetation effects, such a strong $\delta^{13}C$-δD relationship would be unlikely. In that case, there is no clear procedure for correcting for vegetation change.

Some authors have used available data to apply corrections to leaf wax δD records by combining existing $\varepsilon_{l/w}$ data with pollen records (Feakins, 2013) or leaf wax $\delta^{13}C$ (Magill et al., 2013). At LLG though, these correction procedures would underestimate the magnitude of vegetation effects on leaf wax δD because current compilations of $\varepsilon_{l/w}$ values do not accurately represent of the range of vegetation types at this site. In working towards quantitative reconstructions of source water δD, the ideal approach would be to combine detailed information about vegetation composition from pollen or other data with measured $\varepsilon_{l/w}$ values for those taxa (or modern analogues) to produce accurate vegetation corrections. However, this approach requires an extensive and globally representative database of $\varepsilon_{l/w}$ values. An alternative approach would be to target sites with independent constraints on vegetation composition (e.g., high altitude, temperature limitations) that may minimize complications from climate-induced vegetation change.

6. Conclusions

Our results attest to the complexity of the SASM system and the controls on SASM variability over the past 40,000 years. Trends in SASM precipitation in the Pantanal appear to diverge from other regions under glacial conditions, while our record and other SASM records are largely coherent during the Holocene. This discrepancy suggests a redistribution of SASM precipitation during the LGM that additional paleoclimate records and modeling studies could help to resolve. Our record further shows that the Pantanal experienced significant hydrologic changes within the Holocene, possibly due to longer dry seasons during periods of low summer insolation. Elucidating the controls on the seasonality of SASM precipitation is thus another critical direction for future research. Finally, our results also represent an important development

for reconstructions of past hydrologic conditions using leaf wax δD and reveal competing influences on δD signatures at this site. In particular, the effects of vegetation change on leaf wax δD signatures should be considered carefully in future studies as we work towards a better understanding of variability in isotopic fractionation during leaf wax synthesis. The combination of leaf wax δD records with detailed vegetation reconstructions from pollen data or leaf wax $\delta^{13}C$ data can therefore help to improve the robustness of leaf wax δD as a climate proxy.

Acknowledgements

We thank Carl Johnson and Sean Sylva for assistance with isotope analysis. We thank the editor and two anonymous reviewers for comments that helped to improve the manuscript. This work was supported by a U.S. Environmental Protection Agency (EPA) STAR Graduate Fellowship (Assistance agreement FP-91762301-0) and WHOI internal grant to K.L.F. This work has not been formally reviewed by the EPA. The views expressed in this manuscript are solely those of the authors, and the EPA does not endorse any products or commercial services mentioned therein.

References

Alho, C.J.R., 2005. The Pantanal, in: Fraser, L.H., Keddy, P.A. (Eds.), The World's Largest Wetlands: Ecology and Conservation, pp. 203-271.

Assine, M.L., Merino, E.R., Pupim, F.N., Warren, L.V., Guerreiro, R.L., McGlue, M.M., 2015. Geology and Geomorphology of the Pantanal Basin, in: The Handbook of Environmental Chemistry, The Handbook of Environmental Chemistry. Springer Berlin Heidelberg, Berlin, Heidelberg.

Assine, M.L., Silva, A., 2009. Contrasting fluvial styles of the Paraguay River in the northwestern border of the Pantanal wetland, Brazil. Geomorphology 113, 189–199.

Assine, M.L., Soares, P.C., 2004. Quaternary of the Pantanal, west-central Brazil. Quat. Int. 114, 23–34.

Baker, P., Seltzer, G., Fritz, S., Dunbar, R., Grove, M., Tapia, P., Cross, S., Rowe, H., Broda, J., 2001. The history of South American tropical precipitation for the past 25,000 years. Science

291, 640–643.
Bintanja, R., Van De Wal, R.S., Oerlemans, J., 2005. Modeled atmospheric temperatures and global sea levels over the past million years. Nature 437, 125–128.
Bird, B.W., Abbott, M.B., Rodbell, D.T., Vuille, M., 2011. Holocene tropical South American hydroclimate revealed from a decadally resolved lake sediment $\delta^{18}O$ record. Earth Planet. Sci. Lett. 310, 192–202.
Blard, P.-H., Sylvestre, F., Tripati, A., Claude, C., Causse, C., Coudrain, A., Condom, T., Seidel, J.-L., Vimeux, F., Moreau, C., Dumoulin, J.-P., Lavé, J., 2011. Lake highstands on the Altiplano (Tropical Andes) contemporaneous with Heinrich 1 and the Younger Dryas: new insights from ^{14}C, U–Th dating and δ18O of carbonates. Quat. Sci. Rev. 30, 3973–3989.
Bray, E.E., Evans, E.D., 1961. Distribution of *n*-paraffins as a clue to recognition of source beds. Geochim. Cosmochim. Acta 22, 2–15.
Burbridge, R., Mayle, F., Killeen, T., 2004. Fifty-thousand-year vegetation and climate history of Noel Kempff Mercado National Park, Bolivian Amazon. Quaternary Research 61, 215–230.
Burn, M.J., Mayle, F.E., Killeen, T.J., 2010. Pollen-based differentiation of Amazonian rainforest communities and implications for lowland palaeoecology in tropical South America. Palaeogeogr., Palaeoclimatol., Palaeoecol. 295, 1–18.
Bush, M., 2002. On the interpretation of fossil Poaceae pollen in the lowland humid neotropics. Palaeogeogr., Palaeoclimatol., Palaeoecol. 177, 5–17.
Cheng, H., Sinha, A., Cruz, F.W., Wang, X., Edwards, R.L., D Rsquo Horta, F.M., Ribas, C.C., Vuille, M., Stott, L.D., Auler, A.S., 2013. Climate change patterns in Amazonia and biodiversity. Nature Comm. 4, 1411–1416.
Chikaraishi, Y., Naraoka, H., 2003. Compound-specific δD– $\delta^{13}C$ analyses of *n*-alkanes extracted from terrestrial and aquatic plants. Phytochemistry 63, 361–371.
Cook, K.H., Vizy, E.K., 2006. South American climate during the Last Glacial Maximum: Delayed onset of the South American monsoon. J. Geophys. Res 111, D02110.
Cross, S., Baker, P., Seltzer, G., Fritz, S., Dunbar, R., 2000. A new estimate of the Holocene lowstand level of Lake Titicaca, central Andes, and implications for tropical palaeohydrology. The Holocene 10, 21–32.
Cruz, F.W., Burns, S.J., Karmann, I., Sharp, W.D., Vuille, M., Cardoso, A.O., Ferrari, J.A., Silva Dias, P.L., Viana Jr., O., 2005. Insolation-driven changes in atmospheric circulation over the past 116,000 years in subtropical Brazil. Nature 434, 63–66.
Dansgaard, W., 1964. Stable isotopes in precipitation. Tellus 16, 436–468.
Do Amaral, M., Da Silva, A., Salatino, A., 1990. Alkanes of surface waxes from eight species of aquatic angiosperms. Aquat. Bot. 36, 281–286.
Do Prado, A., Heckman, C., Martins, F., 1994. The Seasonal Succession of Biotic Communities in Wetlands of the Tropical Wet-and-Dry Climatic Zone: II. The Aquatic Macrophyte Vegetation in the Pantanal of Mato Grosso, Brazil. Internationale Revue der gesamten Hydrobiologie und Hydrographie 79, 569–589.
Eglinton, G., Hamilton, R., 1967. Leaf epicuticular waxes. Science 156, 1322.
Eglinton, T., Eglinton, G., 2008. Molecular proxies for paleoclimatology. Earth Planet.Sci. Lett. 275, 1–16.
Ehleringer, J., Cerling, T., Helliker, B., 1997. C_4 photosynthesis, atmospheric CO_2, and climate. Oecologia 112, 285–299.
Ehleringer, J.R., Monson, R.K., 1993. Evolutionary and ecological aspects of photosynthetic pathway variation. Ann. Rev. Ecol. Syst. 24, 411–439.

Feakins, S.J., 2013. Pollen-corrected leaf wax D/H reconstructions of northeast African hydrological changes during the late Miocene. Palaeogeogr., Palaeoclimatol., Palaeoecol. 374, 62–71.
Fellerhoff, C., Voss, M., Wantzen, K., 2003. Stable carbon and nitrogen isotope signatures of decomposing tropical macrophytes. Aquat. Ecol. 37, 361–375.
Ficken, K., Li, B., Swain, D., Eglinton, G., 2000. An *n*-alkane proxy for the sedimentary input of submerged/floating freshwater aquatic macrophytes. Org. Geochem. 31, 745–749.
Fornace, K.L., Hughen, K.A., Shanahan, T.M., Fritz, S.C., Baker, P.A., Sylva, S.P., 2014. A 60,000-year record of hydrologic variability in the Central Andes from the hydrogen isotopic composition of leaf waxes in Lake Titicaca sediments. Earth Planet. Sci. Lett. 408, 263–271.
Garcin, Y., Schefuß, E., Schwab, V.F., Garreta, V., Gleixner, G., Vincens, A., Todou, G., Séné, O., Onana, J.-M., Achoundong, G., Sachse, D., 2014. Reconstructing C_3 and C_4 vegetation cover using *n*-alkane carbon isotope ratios in recent lake sediments from Cameroon, Western Central Africa. Geochim. Cosmochim. Acta 142, 482–500.
Garreaud, R., Vuille, M., Compagnucci, R., Marengo, J., 2009. Present-day South American climate. Palaeogeogr., Palaeoclimatol., Palaeoecol. 281, 180–195.
Hamilton, S.K., 2002. Hydrological Controls of Ecological Structure and Function in the Pantanal Wetland (Brazil), in: McClain, M. (Ed.), The Ecohydrology of South American Rivers and Wetlands. International Association of Hydrological Sciences, pp. 133–158.
Kahmen, A., Hoffmann, B., Schefuß, E., Arndt, S.K., Cernusak, L.A., West, J.B., Sachse, D., 2013. Leaf water deuterium enrichment shapes leaf wax *n*-alkane δD values of angiosperm plants II: Observational evidence and global implications. Geochim. Cosmochim. Acta 111, 50–63.
Kanner, L.C., Burns, S.J., Cheng, H., Edwards, R.L., 2012. High-Latitude Forcing of the South American Summer Monsoon During the Last Glacial. Science 335, 570–573.
Knapp, A.K., Medina, E., 1999. Success of C_4 Photosynthesis in the Field: Lessons from Communities Dominated by C_4 Plants, in: Sage, R.F., Monson, R.K. (Eds.), C_4 Plant Biology, pp. 251-283.
Laskar, J., Robutel, P., Joutel, F., Gastineau, M., Correia, A.C.M., Levrard, B., 2004. A long-term numerical solution for the insolation quantities of the Earth. Astron. Astrophys. 428, 261-285.
Liu, Z., Harrison, S.P., Kutzbach, J., Otto-Bliesner, B., 2004. Global monsoons in the mid-Holocene and oceanic feedback. Clim. Dyn. 22, 157–182.
Lüttge, U., 2010. Ability of crassulacean acid metabolism plants to overcome interacting stresses in tropical environments. AoB Plants 2010, plq005.
Magill, C.R., Ashley, G.M., Freeman, K.H., 2013. Water, plants, and early human habitats in eastern Africa. Proc. Nat. Acad. Sci. 110, 1175–1180.
Marzi, R., Torkelson, B.E., Olson, R.K., 1993. A revised carbon preference index. Org. Geochem. 20, 1303–1306.
Mayle, F.E., Burbridge, R., Killeen, T.J., 2000. Millennial-scale dynamics of southern Amazonian rain forests. Science 290, 2291-2294.
Mayle, F.E., Beerling, D.J., Gosling, W.D., Bush, M.B. Responses of Amazonian ecosystems to climatic and atmospheric carbon dioxide changes since the last glacial maximum. Philos. Trans. R. Soc. B 359, 499-514.
Mayle, F.E., Power, M.J., 2008. Impact of a drier Early-Mid-Holocene climate upon Amazonian forests. Philos. Trans. R. Soc. B 363, 1829–1838.

McGlue M.M., Silva, A., Zani, H., Corradini, F.A., Parolin, M., Abel, E.J., Cohen, A.S., Assine, M.L., Ellis, G.S., Trees, M.A., Kuerten, S., dos Santos Gradella, F., Rasbold, G.G., 2012. Lacustrine records of Holocene flood pulse dynamics in the Upper Paraguay River watershed (Pantanal Wetlands, Brazil). Quat. Res. 78: 285–294.

Medina, E., Motta, N., 1990. Metabolism and distribution of grasses in tropical flooded savannas in Venezuela. J. Trop. Ecol. 6, 77–89.

Metcalfe, S.E., Whitney, B.S., Fitzpatrick, K.A., Mayle, F.E., Loader, N.J., Street-Perrott, F.A., Mann, D.G., 2014. Hydrology and climatology at Laguna La Gaiba, lowland Bolivia: complex responses to climatic forcings over the last 25 000 years. J. Quat. Sci. 29, 289–300.

Mosblech, N.A.S., Bush, M.B., Gosling, W.D., Hodell, D., Thomas, L., Calsteren, P.V., Correa-Metrio, A., Valencia, B.G., Curtis, J., Woesik, R.V., 2012. North Atlantic forcing of Amazonian precipitation during the last ice age. Nature Geosci. 5, 817–820.

Pott, A., Oliveira, A.K.M., Damasceno-Junior, G.A., Silva, J.S.V., 2011. Plant diversity of the Pantanal wetland. Braz. J. Biol. 71, 265-273.

Punyasena, S., Mayle, F., McElwain, J., 2008. Quantitative estimates of glacial and Holocene temperature and precipitation change in lowland Amazonian Bolivia. Geology 36, 667.

Rodela, L.G., Queiroz Neto, J.P., Santos, S.A., 2007. Classifição das pastagens nativas do Pantanal da Nhecolandia, Mato Grosso do Sul, por meio de imagens de satellite. Anais XIII Simpósio Brasileiro de Sensoriamento Remoto, Florianópolis, Brasil, 21-26 abril 2007, pp. 4187-4194.

Sachse, D., Billault, I., Bowen, G.J., Chikaraishi, Y., Dawson, T.E., Feakins, S.J., Freeman, K.H., Magill, C.R., Mcinerney, F.A., Van Der Meer, M.T., Polissar, P., Robins, R.J., Sachs, J.P., Schmidt, H.-L., Sessions, A.L., White, J.W., West, J.B., Kahmen, A., 2012. Molecular Paleohydrology: Interpreting the Hydrogen-Isotopic Composition of Lipid Biomarkers from Photosynthesizing Organisms. Ann. Rev. Earth Planet. Sci. 40, 221–249.

Schessl, M., 1999. Floristic composition and structure of floodplain vegetation in the Northern Pantanal of Mato Grosso, Brazil. Phyton (Horn, Austria) 39, 303-336.

Sessions, A.L., Burgoyne, T.W., Hayes, J.M., 2001. Determination of the H3 factor in hydrogen isotope ratio monitoring mass spectrometry. Anal. Chem. 73, 200–207.

Still, C.J., 2003. Global distribution of C_3 and C_4 vegetation: Carbon cycle implications. Global Biogeochem. Cycles 17, 1006.

Vizy, E., Cook, K., 2007. Relationship between Amazon and high Andes rainfall. J. Geophys. Res. 112, D07107.

Vuille, M., Bradley, R.S., Werner, M., Healy, R., Keimig, F., 2003. Modeling $\delta^{18}O$ in precipitation over the tropical Americas: 1. Interannual variability and climatic controls. J. Geophys. Res. 108, 4174.

Vuille, M., Werner, M., 2005. Stable isotopes in precipitation recording South American summer monsoon and ENSO variability: observations and model results. Clim. Dyn. 25, 401–413.

Wang, X., Auler, A.S., Edwards, R.L., Cheng, H., Ito, E., Wang, Y., Kong, X., Solheid, M., 2007. Millennial-scale precipitation changes in southern Brazil over the past 90,000 years. Geophys. Res. Lett 34, L23701.

Wantzen, K., de Arruda Machado, F., Voss, M., Boriss, H., Junk, W., 2002. Seasonal isotopic shifts in fish of the Pantanal wetland, Brazil. Aquat. Sci. 64, 239–251.

Whitney, B., Mayle, F., Punyasena, S., Fitzpatrick, K., Burn, M., Guillen, R., Chavez, E., Mann, D., Pennington, R., Metcalfe, S., 2011. A 45 kyr palaeoclimate record from the lowland interior of tropical South America. Palaeogeogr., Palaeoclimatol., Palaeoecol. 307, 177-192.

Whitney, B.S., Mayle, F.E., 2012. Pediastrum species as potential indicators of lake-level change in tropical South America. J. Paleolimnol. 47, 601–615.
Zhou, J., Lau, K., 1998. Does a monsoon climate exist over South America? J. Clim. 11, 1020-1040.

Table 1. Surface sediment *n*-alkane $\delta^{13}C$ and δD values (‰).

Compound	Core site				Paraguay River margin sediment			
	$\delta^{13}C$	σ	δD	σ	$\delta^{13}C$	σ	δD	σ
n-C_{27}	-32.1	0.2	---	---	-31.0	0.1	---	---
n-C_{29}	-31.2	0.1	-167	3.2	-31.0	0.1	-175	2.4
n-C_{31}	-30.7	0.3	-170	2.6	-31.3	0.1	-180	3.7
n-C_{33}	-29.3	0.1	-172	1.9	-29.8	0.1	-182	6.3

Table 2. Coefficients of determination (r^2) for linear regressions between $ACL_{25\text{-}35}$, $\delta^{13}C$ values and graminoid pollen abundance from 41-20 ka. P values are shown in parentheses.

	$ACL_{25\text{-}35}$	Graminoid Pollen
n-C_{27} $\delta^{13}C$	0.61 (0.002)	0.70 (<0.001)
n-C_{29} $\delta^{13}C$	0.60 (0.002)	0.58 (0.003)
n-C_{31} $\delta^{13}C$	0.54 (0.004)	0.56 (0.001)
n-C_{33} $\delta^{13}C$	0.39 (0.02)	0.48 (0.008)
$ACL_{25\text{-}35}$	---	0.69 (<0.001)

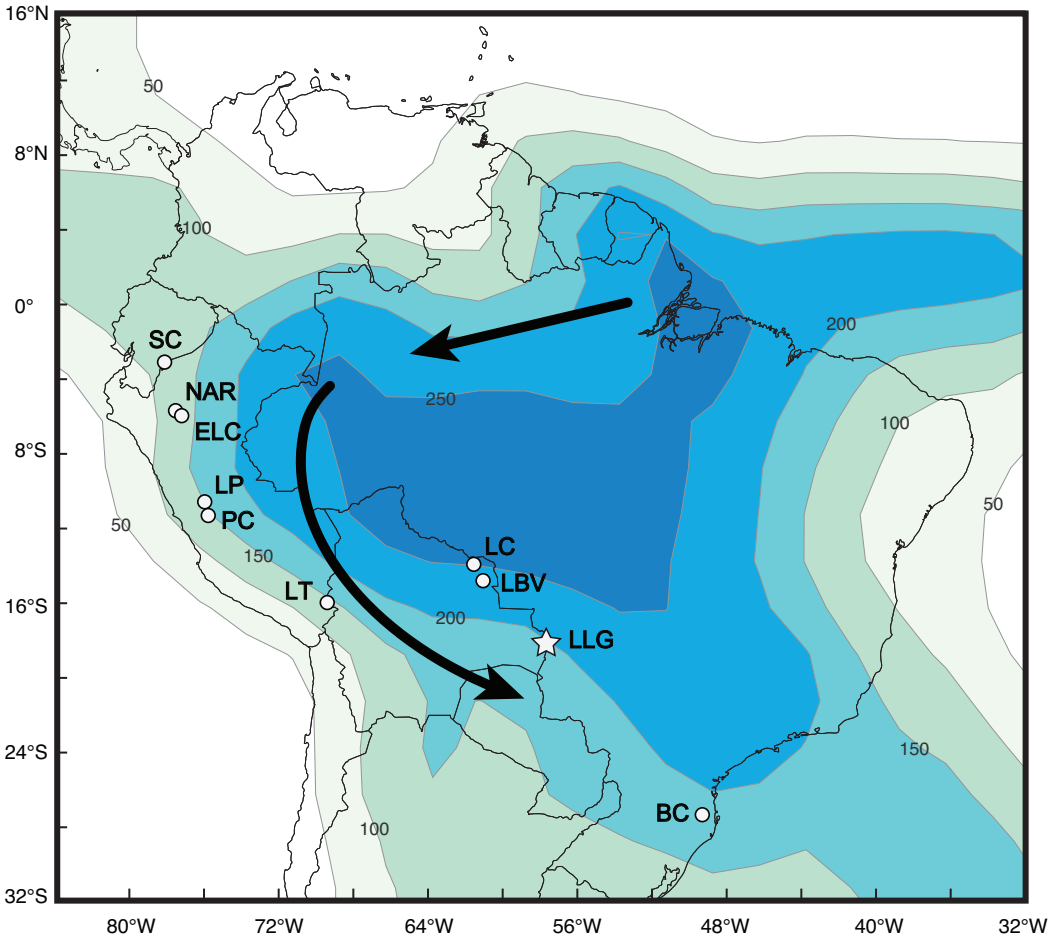

Figure 1. Map of South American tropics with sites discussed in text and average January precipitation (mm/month, 1981-2010). Contours indicate increments of 50 mm/month; precipitation data are from CAMS_OPI monthly precipitation dataset (NCEP). Study site Laguna La Gaiba (LLG) is marked with a star; other sites include Santiago Cave (SC; Mosblech et al., 2012), Cueva del Diamante/El Condor (NAR/ELC; Cheng et al., 2013), Laguna Pumacocha (LP; Bird et al., 2011), Pacupahuain Cave (PC; Kanner et al., 2012), Lake Titicaca (LT; Fornace et al., 2014, Baker et al., 2001), Laguna Chaplin/Laguna Bella Vista (LC/LBV; Mayle et al., 2000, Burbridge et al., 2004), and BC (Botuverá Cave; Cruz et al., 2005, Wang et al., 2007). Arrows indicate general direction of moisture transport from tropics to subtropics during monsoon season.

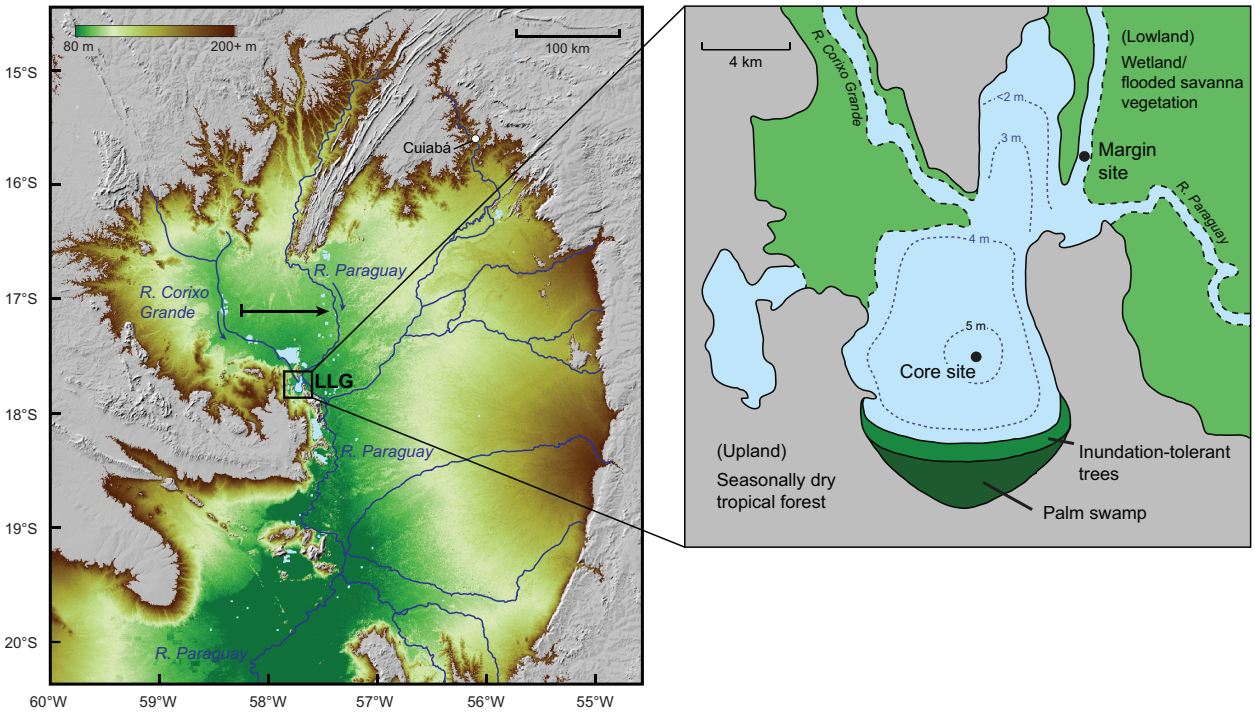

Figure 2. Elevation map of Pantanal basin (left) and schematic of modern configuration of Laguna La Gaiba and surrounding vegetation (right). Elevation map with constructed with SRTM3 Digital Elevation Model (NASA). Black arrow in left panel shows past migration of main stem of Paraguay River as reconstructed by Assine and Silva (2009), while blue arrows show direction of river flow. Right panel was adapted from Whitney et al. (2011). Locations of core site and margin surface sediment collection site are shown by black circles in right panel.

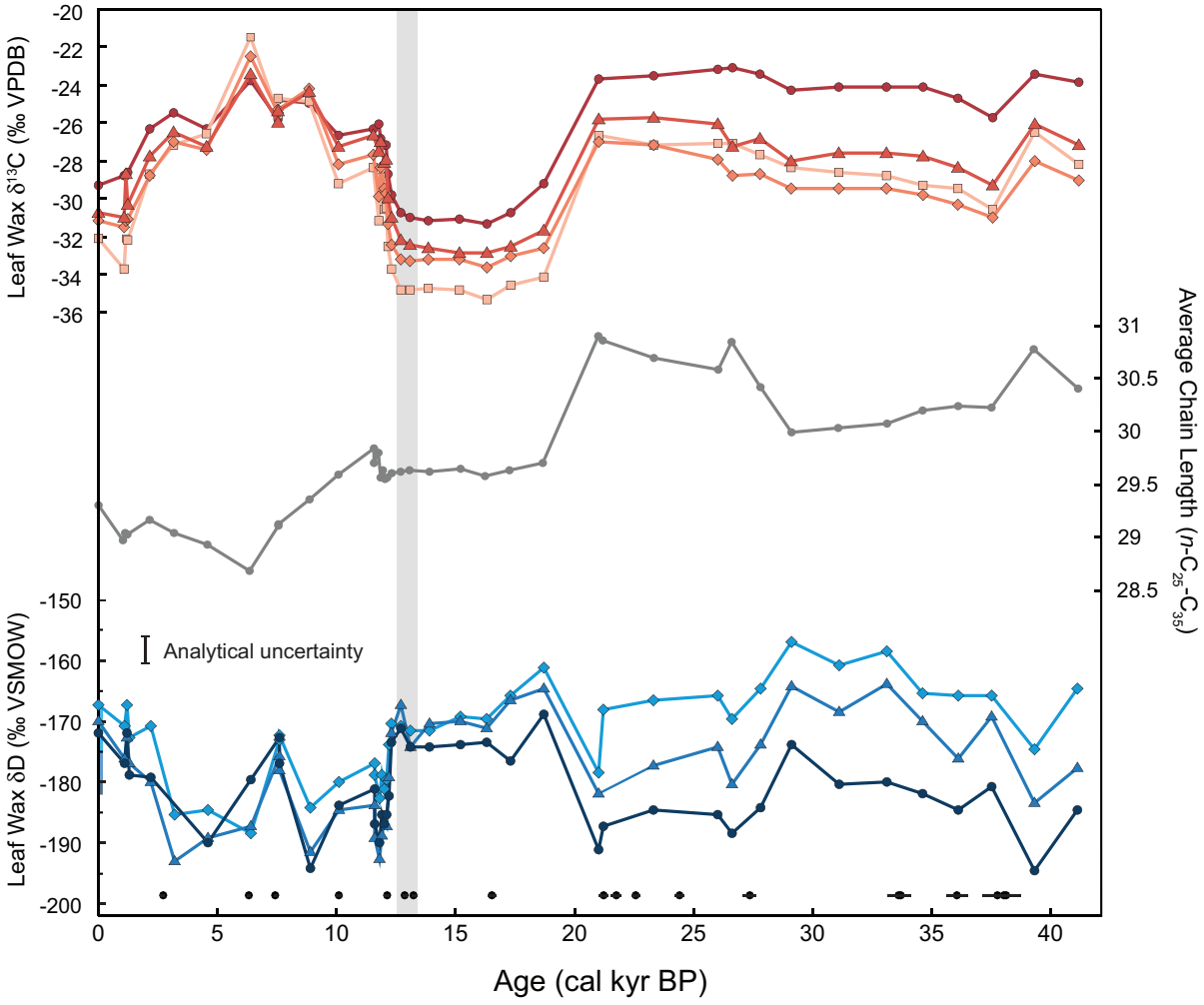

Figure 3. Time series of LLG *n*-alkane $\delta^{13}C$ (top), average chain length (middle), and δD (bottom) over past 40 kyr. Isotopic data are shown for *n*-C_{27} (squares, $\delta^{13}C$ only), *n*-C_{29} (diamonds), *n*-C_{31} (triangles), and *n*-C_{33} (circles). Average analytical uncertainty for $\delta^{13}C$ measurements was smaller than the size of symbols; average analytical uncertainty for δD is indicated by error bar on bottom plot. Errors for individual points are not shown in order to reduce the complexity of the plots but are provided in dataset archived online. Bars at 0 ka on the δD time series indicate range of δD values measured for *n*-alkanes from two surface sediment samples. Black symbols on bottom plot denote age points derived from 17 terrestrial macrofossil and two sediment organic carbon radiocarbon dates used to construct core chronology (Whitney et al., 2011). Gray shaded bar indicates approximate timing of abrupt ~5-10-fold increase in lake sedimentation rate.

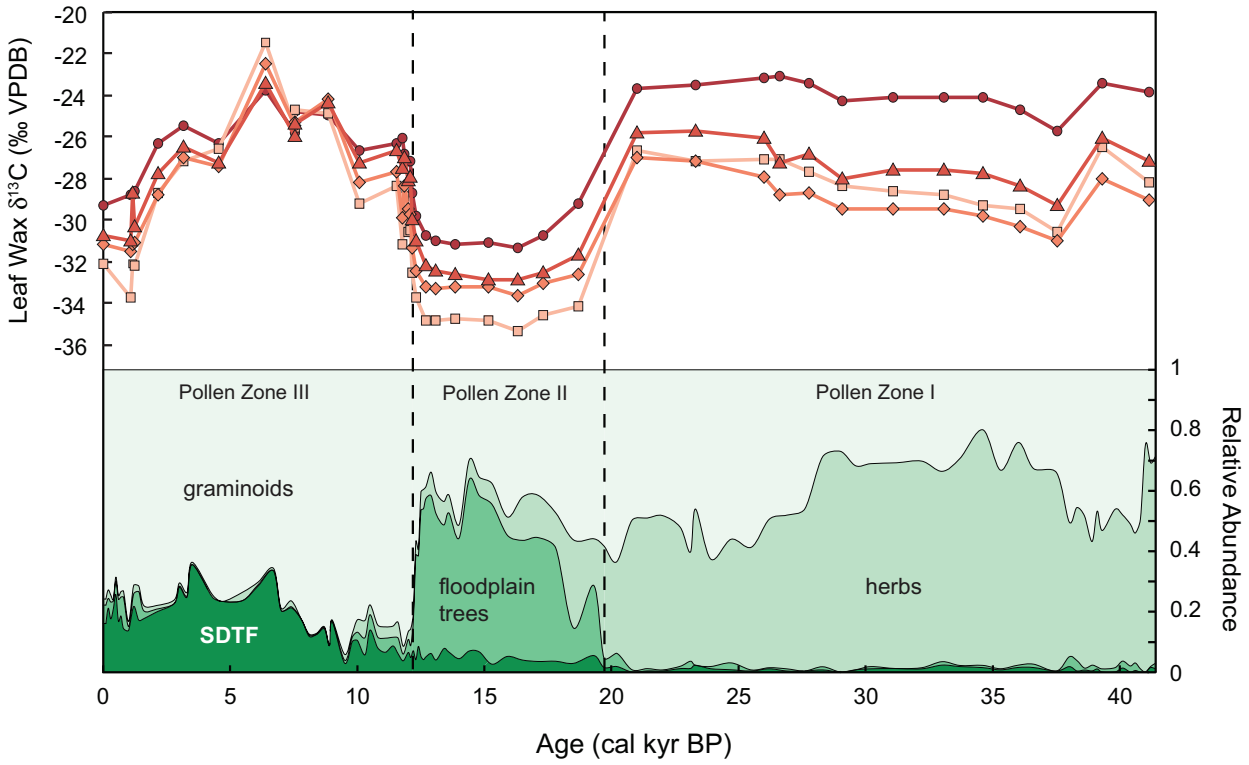

Figure 4. Comparison of LLG *n*-alkane $\delta^{13}C$ (top) and abundance of major vegetation groups from pollen data (bottom) over past 40 kyr. $\delta^{13}C$ values are shown for *n*-C_{27} (squares), *n*-C_{29} (diamonds), *n*-C_{31} (triangles), and *n*-C_{33} (circles). Vegetation types, in order of lightest to darkest shading, include graminoids, herbs, floodplain trees, and seasonally dry tropical forest (SDTF). Dashed lines indicate transitions between pollen zones as defined by Whitney et al. (2011).

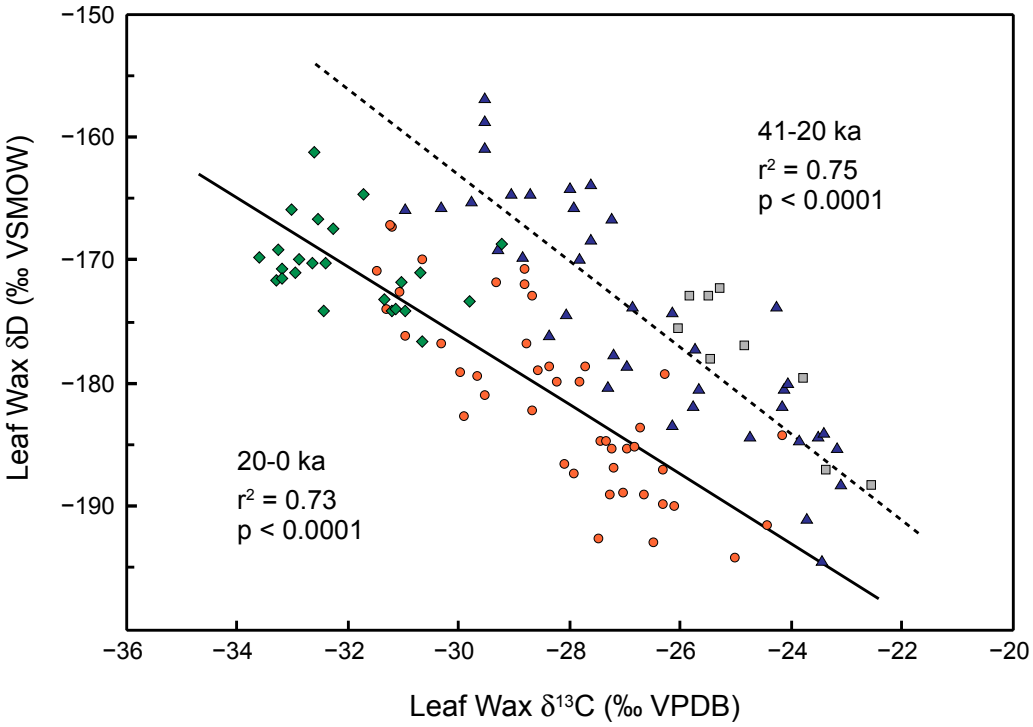

Figure 5. Comparison of all downcore *n*-C_{29}, *n*-C_{31} and *n*-C_{33} alkane $\delta^{13}C$ and δD values. Full glacial (41-20 ka) points are shown as blue triangles, late glacial (20-12.2 ka) as green diamonds, early/mid-Holocene (7.6-6.4 ka) as gray squares, and remaining Holocene (12.2-8.9 ka, 4.6-0 ka) as orange circles. Correlations for 41-20 ka and 20-0 ka are shown by dashed line and solid line, respectively. Note that correlation for 20-0 ka excludes early/mid-Holocene points (see text for further explanation).

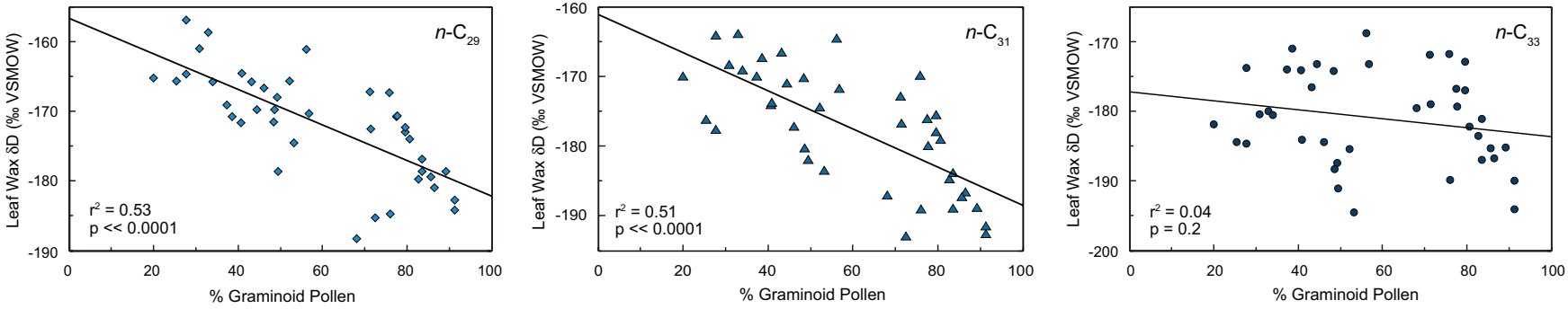

Figure 6. Comparison of *n*-alkane δD values and graminoid (*Poaceae* + *Cyperaceae*) pollen abundance for all downcore samples. From left to right: *n*-C_{29}, *n*-C_{31}, *n*-C_{33} data.

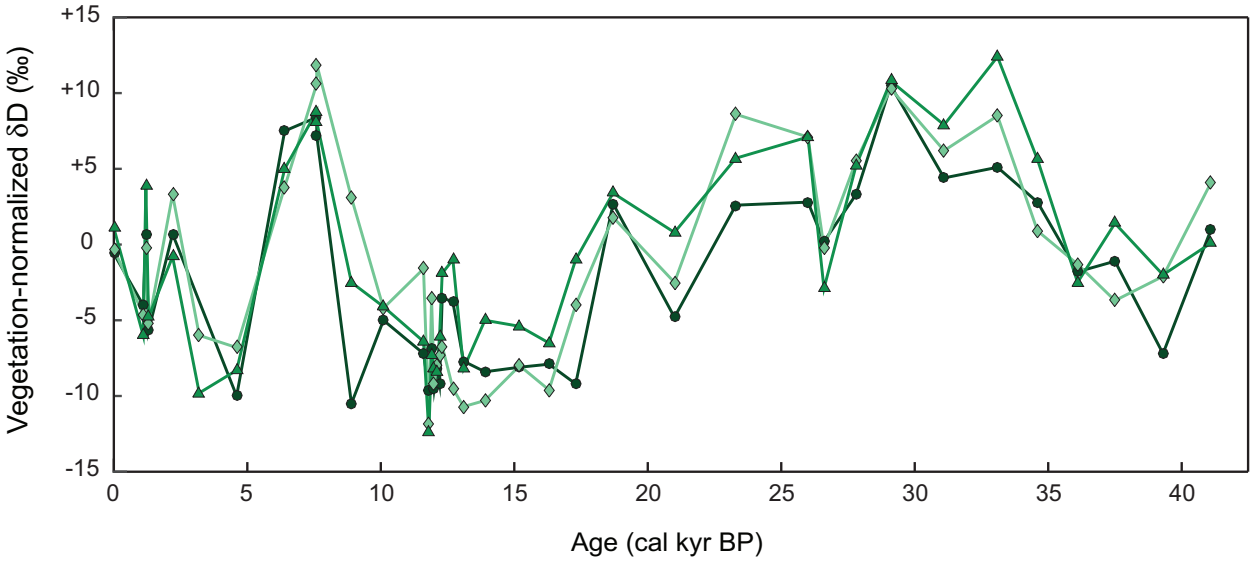

Figure 7. Time series of relative changes in vegetation-normalized δD values (δD_{vn}) for C_{29}-C_{33} *n*-alkanes at LLG over the past 40 kyr. δD values were corrected for vegetation change by normalizing values to a pure C_4 endmember using 41-20 ka and 20-0 ka $\delta^{13}C$-δD trends. *n*-C_{29} δD_{vn} values are shown in light green diamonds, *n*-C_{31} in medium green triangles and *n*-C_{33} in dark green circles.

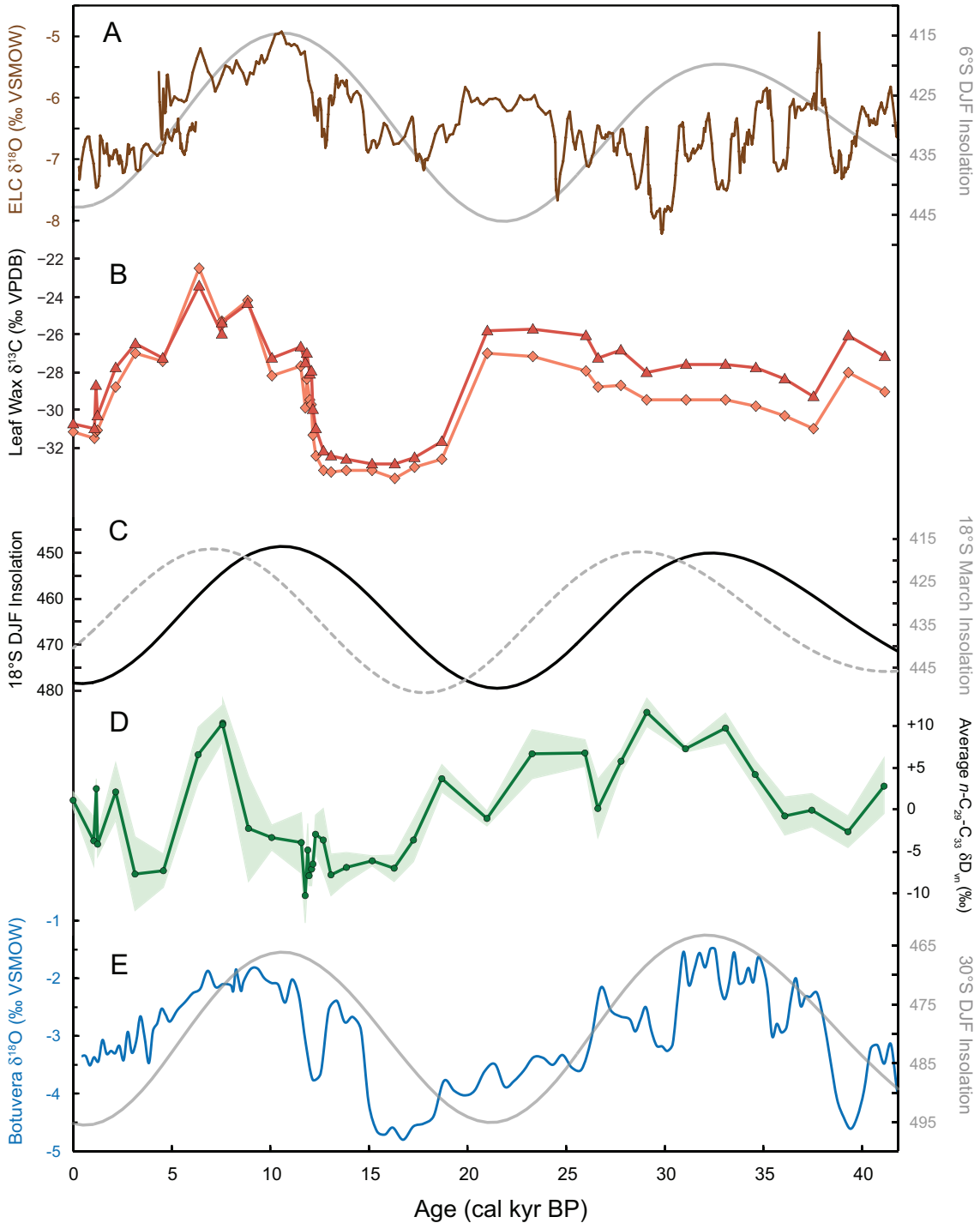

Figure 8. Time series of LLG *n*-alkane $\delta^{13}C$ and δD values and other tropical South American climate records over the past 40 kyr. A. El Condor speleothem $\delta^{18}O$ (western Amazon; Cheng et al., 2013) and mean 6°S summer (DJF) insolation. B. LLG C_{29} (diamonds) and C_{31} (triangles) *n*-alkane $\delta^{13}C$. C. Mean 18°S DJF insolation (black solid line) and March insolation (dotted gray line). D. Relative changes in average vegetation-normalized δD for *n*-C_{29}-C_{33}. Standard deviation (1σ) of average *n*-C_{29}-C_{33} values is shown by light green shading. E. Botuverá Cave speleothem $\delta^{18}O$ (southern Brazil; Wang et al., 2007) and mean 30°S DJF insolation. Note that for all plots insolation axes are reversed (increasing down). Insolation values were calculated according to Laskar et al. (2004).

Supplementary material

Appendix: additional sample preparation details

Sediment samples (~1-10 g) were freeze-dried and finely ground, and lipids were extracted with a 9:1 dichloromethane:methanol mixture using either an accelerated solvent extractor (ASE 200, Dionex) or microwave-assisted reaction system (MARS, CEMS corporation). Lipid extracts were dried over sodium sulfate and separated into hydrocarbon and polar fractions using 1% deactivated silica gel in Pasteur pipette columns (filled to 4 cm) using 5 mL hexane and 10 mL dichloromethane:methanol (1:1) as eluents, respectively.

n-Alkanes were further purified from the hydrocarbon fraction by urea adduction and $AgNO_3$-impregnated silica gel column chromatography. For urea adduction, 0.5 mL of a solution of urea in methanol (40 mg/mL) was added to *n*-alkanes dissolved in 1.5 mL 2:1 hexane:dichloromethane. The mixture was dried under nitrogen at room temperature, allowing urea crystals to form. The adduction procedure was repeated a total of three times, each time adding 1.5 mL 2:1 hexane:dichloromethane followed by 0.5 mL of the urea solution. After the final adduction, crystals were rinsed three times with 4 mL hexane to remove non-adducts. Urea crystals were then dissolved in 25 mL MilliQ water, and adducts (including *n*-alkanes) were extracted five times with 5 mL 4:1 hexane:dichloromethane. Silver ion chromatography was performed in Pasteur pipette columns with 4 cm $AgNO_3$-impregnated silica gel (Sigma Aldrich). Saturated and unsaturated hydrocarbons were eluted with 4.5 mL hexane and 6 mL dichloromethane, respectively.

Compounds were identified by comparison of gas chromatograph/flame ionization detector (GC/FID, Agilent 5890) retention times to those of authenticated external standards.